7. Goldreich, P., Tremaine, S. & Borderies, N. Towards a theory for Neptune's arc rings. *Astron. J.* **92,** 490–494 (1986).
8. Horanyi, M. & Porco, C. C. Where exactly are the arcs of Neptune? *Icarus* **106,** 225–235 (1993).
9. Dumas, C., Terrile, R. J., Smith, B. A., Schneider, G. H. & Becklin, E. E. Stability of Neptune's ring arcs in question. *Nature* **400,** 733–735 (1999).
10. Owen, W. M. Jr, Vaughan, R. M. & Synnott, S. P. Orbits of the six new satellites of Neptune. *Astron. J.* **101,** 1511–1515 (1991).
11. Roddier, C. *et al.* Satellites and rings of Neptune. *IAU Circ.* No. 7051 (1998).
12. Foryta, D. W. & Sicardy, B. The dynamics of the Neptunian Adams ring's arcs. *Icarus* **123,** 129–167 (1996).
13. Lissauer, J. J. Shepherding model for Neptune's arc ring. *Nature* **318,** 544–545 (1985).
14. Hänninen, J. & Porco, C. Collisional simulations of Neptune's ring arcs. *Icarus* **126,** 1–27 (1997).
15. Graves, J. E., Northcott, M., Roddier, F., Roddier, C. & Close, L. First light for Hokupa'a, 36-element curvature optics system at UH. *Proc. SPIE* **3353,** 34–43 (1998).
16. Roddier, F., Northcott, M. & Graves, J. E. A simple low-order adaptive optics system for near-infrared applications. *Publ. Astron. Soc. Pacif.* **103,** 131–149 (1991).
17. Roddier, F. Curvature sensing and compensation: a new concept in adaptive optics. *Appl. Opt.* **27,** 1223–1225 (1988).
18. Roddier, C. *et al.* Rings of Neptune. *IAU Circ.* No. 7108 (1999).
19. Jacobson, R. A., Riedel, J. E. & Taylor, A. H. The orbits of Triton and Nereid from spacecraft and earthbased observations. *Astron. Astrophys.* **247,** 565–575 (1991).

Acknowledgements. The work of E.P. at DESPA is supported by the G. Colombo research fellowship of the European Space Agency. Adaptive optics observations of Neptune at the University of Hawaii were supported by NASA.

Correspondence and requests for materials should be addressed to B.S. (e-mail: Bruno.Sicardy@obspm.fr).

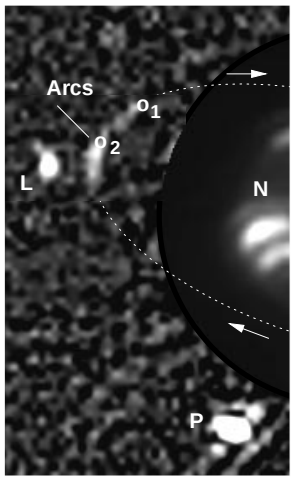

Figure 1 Initial image of Neptune's ring arcs obtained by the HST and its near-infrared camera NICMOS on 3 June 1998 at 19:40 UT. We used camera 2 (~0.076 arcsec per pixel) to image the vicinity of Neptune at 1.87 μm while the planet's phase and aspect angles were respectively 1.9 and 63 degrees. Neptune's disk was positioned partly outside the field of view of the camera to reduce the scattered light coming from the planet. In this image, Neptune's contribution to the background has been modelled and removed. An image of Neptune's clouds has been superimposed for better clarity of the system geometry. The two circles (labelled 1 and 2) correspond to the positions of the middle-point of the trailing Egalité arc derived from the two possible solutions[7] for the arcs' mean motion: $n_1 = 820.1194\,\mathrm{deg\,d^{-1}}$ and $n_2 = 820.1118\,\mathrm{deg.\,d^{-1}}$. The letters L, P and N mark respectively the positions of Larissa, Proteus and Neptune, and the arrow shows the direction of motion of the ring arcs along their orbit. The measured location of the trailing Egalité arc fits better the position obtained with the mean-motion solution n_2 than n_1.

Stability of Neptune's ring arcs in question

Christophe Dumas*, Richard J. Terrile*, Bradford A. Smith†, Glenn Schneider‡ & E. E. Becklin§

* *Jet Propulsion Laboratory, 4800 Oak Grove Drive, MS 183-501, Pasadena, California 91109-8099, USA*
† *University of Hawaii, Institute for Astronomy, 82-6012 Pu'uhonua Road, Napo'opo'o, Hawaii 96704, USA*
‡ *University of Arizona, Steward Observatory, 933 N. Cherry Avenue, Tucson, Arizona 85721, USA*
§ *University of California at Los Angeles, Department of Physics and Astronomy, 405 Hilgard Avenue, Los Angeles, California 90095-1562, USA*

Although all four of the gas-giant planets in the Solar System have ring systems, only Neptune exhibits 'ring arcs'—stable clumps of dust that are discontinuous from each other[1]. Two basic mechanisms for confining the dust to these arcs have been proposed. The first[2] relies on orbital resonances with two shepherding satellites, while the second[3] invokes a single satellite (later suggested to be Galatea[4]) to produce the observed ring arc structures. Here we report observations of the ring arcs and Galatea, which show that there is a mismatch between the locations of the arcs and the site of Galatea's co-rotation inclined resonance. This result calls into question Galatea's sole role in confining the arcs.

A new determination of the mean motion of the arcs was made possible by the Hubble Space Telescope (HST), using the Near Infrared Camera Multi-Object Spectrometer[5] (NICMOS), which observed the system of Neptune's faint arcs on two occasions in 1998. To aid in the rejection of background light at the radial angular distance of the ring arcs (~3 arcsec) from the planet centre, a filter with a bandpass centred at 1.87 μm wavelength was used. This wavelength corresponds to a strong absorption in the reflective spectrum of methane, one of the main constituents of Neptune's atmosphere. The projected azimuthal resolution was 3.2 degrees per resolution element (1.6 degrees per pixel) at the distance of the Adams ring, which corresponds to a resolution of 3,500 km along the ring. The first images of the arcs since the Voyager fly-by[6] were obtained by NICMOS on 3 June 1998. The arcs were clearly detected at the maximum of eastern elongation (Fig. 1) during a single 832-s exposure. The orbital motion of the arcs smeared the image by 8 degrees along the azimuthal direction; this is about the full length of the longest arc, Fraternité. Nevertheless, the mean motion was unambiguously determined to be very close to the proposed value (or 'solution') of $820.1118\,\mathrm{deg.\,d^{-1}}$ (ref. 7). Before these observations, another solution ($820.1194\,\mathrm{deg\,d^{-1}}$) was preferred because it supported better the action of the 42:43 co-rotation inclined resonance (CIR) with Galatea[4].

We then modified our observational strategy to improve the image quality and spatial resolution for the two remaining HST orbits. Additional NICMOS observations were obtained on 20 and 22 October 1998. An image of the system of ring arcs is given in Fig. 2, as seen by an observer viewing from the ring-plane normal. The arcs extend over 40.7 ± 3.3 degrees and the brightest trailing arcs, Egalité and Fraternité, are clearly seen. The faintest leading arcs, Courage and Liberté, are just above the noise-level (3.5σ above background for Courage, the faintest arc). The centre of Egalité was used as a fiducial point to measure the locations of the ring arcs. The arcs were found to be 0.8 ± 1.5 degrees ahead of the ephemerides prediction employing a mean motion of $820.1118\,\mathrm{deg\,d^{-1}}$. This measurement confirmed without ambiguity the results obtained during the June 1998 observations[8]. The new value for the arcs' mean motion is $820.1120 \pm 0.0004\,\mathrm{deg\,d^{-1}}$. Similarly, we determined a revised mean motion for Galatea of $839.6617 \pm 0.0004\,\mathrm{deg\,d^{-1}}$.

The brightness profile in backscattered light (Fig. 3) was obtained by integrating the flux, radially, over the photometric width of the arcs. Following the practice employed in earlier studies of Neptune's rings[6,9], we measured the equivalent width E_i seen by NICMOS in the optically thin case. Assuming that the optical depth of Egalité has not changed since 1989, its equivalent width, E_i, and geometric albedo, $p_{1.87\,\mu m}$, are 45 ± 5 m and 0.048 ± 0.005, respectively. The letter is very close to that measured by Voyager at visible wavelength ($p_{0.5\,\mu m} = 0.055 \pm 0.004$), demonstrating that the colour of the material making up the ring arcs is similar to that in the rings of

Uranus[10]; that is, very dark with a relatively flat spectral reflectivity. Comparison between the HST brightness profile and the Voyager profile obtained at high phase angle (135°) shows that the apparent structure of the arcs has remained roughly the same since 1989. The main change concerns Liberté, which appears to be displaced from its position relative to Egalité by about 1.9 degrees in the leading direction. We assume that this shift cannot be solely caused by differences in the particle size distribution in Liberté, as the Voyager results showed similar brightness ratios among the three widest arcs at high and low phase angles.

Without stabilizing external forces, keplerian shear would spread the material of the ring arcs along the orbit of the Adams ring in a matter of a few months. The model of a single satellite responsible for both the radial and azimuthal confinement of the ring-arcs' material was first proposed in 1986 by Goldeich *et al.*[3]. This theory was supported by the work of Porco *et al.*[4,11] who showed that Galatea, orbiting at the inner edge of the Adams ring on a slightly inclined trajectory (0.0544 degrees; ref. 12), was the most plausible body responsible for the long-lived stability of the arcs. The satellite would be responsible for the radial confinement of the dust through its 42:43 Linblad resonance (this mechanism was confirmed by Voyager observations of a 30-km radial distortion attributed to the Linblad resonance with Galatea). At the same time, its 42:43 CIR would prevent the arc material from spreading azimuthally. The relation between the motions of the CIR site and Galatea is defined as $m_c n_{CIR} = (m_c - 1)n_G + \dot{\Omega}$, where $\dot{\Omega}$ is Galatea's nodal precession rate, n_G the motion of Galatea, and m_c is the co-rotation resonance wavenumber. The location of the CIR produced by Galatea that falls closest to the arcs' semi-major axis is obtained for $m_c = 43$. Assuming that the value of $\dot{\Omega}$ determined by Voyager[12] remains unchanged—which is reasonable since Galatea's nodal precession rate is essentially determined by Neptune's gravitational harmonics—our new determination of the mean motions of Galatea and the ring arcs position the arcs 311 ± 41 m away from the middle of the CIR site. If we adopt a value for the half-width of the resonance site of 250 m (ref. 13), the mean semi-major axis of the arcs is located outside the region defined by the CIR with Galatea. This measurement calls into question the unique role of Galatea in confining azimuthally the material inside the arcs, leaving the field open for alternative models. We note that the wider (9 km; ref. 4) Linblad resonance remains a valid process to provide the arcs with the required energy to maintain their radial confinement.

Another possible scheme, as suggested originally by Lissauer[2], relies on two satellites instead of one. Although this model is based on the presence of an hypothetical moonlet co-orbiting with the Adams ring and responsible for trapping the dust between its L_4 and L_5 lagrangian points, it would solve the problem raised by the two trailing arcs Egalité and Fraternité that have widths well over the length (4.186 degrees) predicted by the 42:43 CIR with Galatea. Our

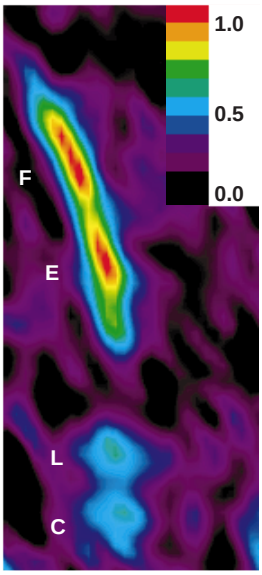

Figure 2 Higher-resolution false-colour image of the four ring arcs of Neptune obtained by HST/NICMOS at a wavelength of 1.87 μm. A total of 22 dithered images of 208 s each were recorded on 20 June 1998 (12:27 UT) and 22 October 1998 (17:40 UT). A prediction of 0.02 pixel (1.5 mas) in the co-registration of the images by cubic convolution interpolation was achieved by minimizing the difference in the diffraction pattern of Neptune in adjacent images. A model of the planet's scattered light was subtracted from the individual images in order to (1) recover a background level close to zero at the distance of the arcs from Neptune's centre, and (2) eliminate stray light produced by the secondary mirror support structure. The signal produced by the brightest arcs (Egalité/Fraternité) was at the noise level (0.065 μJy per pixel) in the individual images. The arcs were extracted from the individual images by taking into account their motion in the planetocentric reference system linked to Neptune. During the co-registration process, the data were resampled by a factor of two onto a finer grid by cubic convolution interpolation. The physical centre point of the system of satellites and arcs was determined by using the inner neptunian satellites (Proteus, Larissa, Despina and Galatea) present in our images to fit their individual trajectory whose pole solution has been known[12] since Voyager. The immediate benefit of the recentring, shifting and adding processes was to increase the resolution of our images to a point where the error of our measurement of the position of the arcs along the Adams ring was reduced to ±1.5 degrees. The letters C, L, E and F indicate, from leading to trailing, the respective location of the arcs Courage, Liberté, Egalité and Fraternité. The colour has been scaled so the brightest arc has a value of unity.

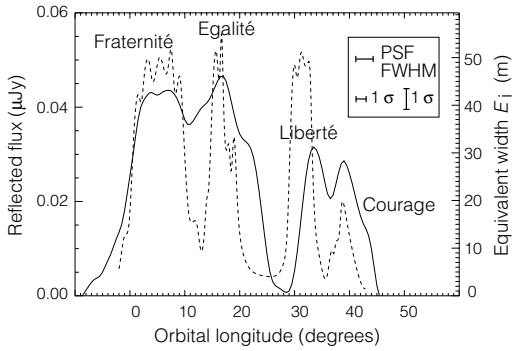

Figure 3 Brightness profile of the arcs along the azimuthal direction. The azimuthal profile of the arcs derived from Fig. 2 is shown here (solid line) both as the NICMOS radially integrated flux in μJy per azimuthal degree and as the equivalent width (E_i) in metres. Relative brightness of the arcs from Voyager (1989) observations, normalized to $E_i = 52$ m (ref. 9) at Egalité, has been overplotted (dashed line) for comparison. We note that the Voyager profile was derived from an image recorded at a relatively high phase angle (135 degrees), where the observed brightness of the arcs is dominated by forward scattering from microscopic dust particles. However, within the measurement uncertainties, the same overall structure was seen in both low and high phase angle Voyager images. The 1σ uncertainties in both the NICMOS observed flux and azimuthal position are also indicated as well as the width (full-width at half-maximum, FWHM) of the NICMOS point-spread function (PSF) at 1.87 μm. The 1σ uncertainty in flux comes from the uncertainty in the determination of the residual background level introduced by the proximity of Neptune. The total integrated flux at 1.87 μm for all of the arcs is 27.0 ± 0.27 μJy, or $M_{1.87\,\mu m} = 21.2 \pm 0.1$ mag. The NICMOS calibration numbers used for filter Nic2/F187W are: conversion factor = 3.819 μJy per data number (DN) per s and zero-magnitude point = 828 Jy. The most apparent changes in the ring-arcs' morphology since 1989 are the widening of Egalité and the decrease in amplitude of Liberté. An effect induced by different scattering properties between high and low phase angles is not likely but cannot be entirely ruled out.

HST observations, along with the ground-based results presented elsewhere in this issue[14], show that the new generation of large telescopes should allow us to collect additional measurements that will be valuable in constraining the theories of ring-arc formation around Neptune. □

Received 18 March; accepted 6 July 1999.

1. Hubbard, W. B. *et al.* Occultation detection of a neptunian ring-like arc. *Nature* **319,** 636–640 (1986).
2. Lissauer, J. J. Shepherding model for Neptune's arc ring. *Nature* **318,** 544–545 (1985).
3. Goldreich, P., Tremaine, S. & Borderies, N. Towards a theory for Neptune's arc rings. *Astron. J.* **92,** 490–494 (1986).
4. Porco, C. C. An explanation for Neptune's ring arcs. *Science* **253,** 995–1001 (1991).
5. Thompson, R. I., Rieke, M., Schneider, G., Hines, D. C. & Corbin, M. Initial on-orbit performance of NICMOS. *Astrophys. J.* **492,** L95–L97 (1998).
6. Smith, B. A. *et al.* Voyager 2 at Neptune: Imaging science results. *Science* **246,** 1422–1449 (1989).
7. Nicholson, P. D., Mosqueira, I. & Matthews, K. Stellar occultation observations of Neptune's rings. *Icarus* **113,** 295–330 (1995).
8. Terrile, R. J. *et al.* First infrared imaging of the Neptune ring arcs: HST/NICMOS results. *Bull. Am. Astron. Soc.* **30,** 1044 (1998).
9. Porco, C. C., Nicholson, P. D., Cuzzi, J. F., Lissauer, J. J. & Esposito, L. W. in *Neptune and Triton* (ed. Cruikshank, D. P.) 703–806 (Univ. Arizona Press, Tucson, 1985).
10. Elliot, J. L. & Nicholson, P. D. in *Planetary Rings* (eds Greenberg, R. & Brahic, A.) 25–72 (Univ. Arizona Press, Tucson, 1984).
11. Horany, M. & Porco, C. C. Where exactly are the arcs of Neptune? *Icarus* **106,** 525–535 (1993).
12. Owen, W. M., Vaughan, R. M. & Synnott, S. P. Orbits of the six new satellites of Neptune. *Astron. J.* **101,** 1511–1515 (1991).
13. Foryta, D. W. & Sicardy, B. The dynamics of the neptunian Adams ring's arcs. *Icarus* **123,** 129–167 (1996).
14. Sicardy, B. *et al.* Images of Neptune's ring arcs obtained by a ground-based telescope. *Nature* **400,** 731–733 (1999).

Acknowledgements. We thank R. Thompson and M. Rieke from the NICMOS IDT team as well as P. Nicholson for calculating the predicted offsets of the arcs for 20 and 22 October 1998, and R. Jacobson for providing us with the coordinates of the normal of the orbital planes of the neptunian inner satellites.

Correspondence and requests for materials should be addressed to C.D. (e-mail: Christophe.Dumas@pl.-nasa.gov).

Linking insulator-to-metal transitions at zero and finite magnetic fields

Y. Hanein*, N. Nenadovic*, D. Shahar*, Hadas Shtrikman*, J. Yoon†, C. C. Li† & D. C. Tsui†

* *Department of Condensed Matter Physics, Weizmann Institute, Rehovot 76100, Israel*
† *Department of Electrical Engineering, Princeton University, Princeton, New Jersey 08544, USA*

For many years, it was widely accepted[1] that electrons confined to two dimensions would adopt an insulating ground state at zero temperature and in zero magnetic field. Application of a strong perpendicular magnetic field changes this picture, resulting[2,3] in a transition from the insulating phase to a metallic quantum Hall state. Unexpectedly, an insulator-to-metal transition was recently observed[4] in high-quality two-dimensional systems at zero magnetic field on changing the charge carrier density. The mechanism underlying this transition remains unknown[5–9]. Here we investigate the magnetic-field-driven transition in a two-dimensional gallium arsenide system, which also exhibits[10–12] the poorly understood zero-field transition. We find that, on increasing the carrier density, the critical magnetic field needed to produce an insulator-to-metal transition decreases continuously and becomes zero at the carrier density appropriate to the zero-field transition. Our results suggest that both the finite- and zero-magnetic field transitions share a common physical origin.

In Fig. 1a we plot the resistivity (ρ) of one of our samples as a function of magnetic field (B) at several temperatures, with the density of holes (p) held fixed. The sample is a p-type, inverted semiconductor–insulator–semiconductor (ISIS) sample[13] grown on the (311)A GaAs substrate[14] with silicon as a p-type dopant. At $B = 0$ the system is insulating, as indicated by a rapidly increasing ρ as the temperature (T) approaches zero. The insulating behaviour is maintained for $B < B_c^L$. For $B > B_c^L$, a quantum-Hall (QH) state ($\nu = 1$, where ν is the Landau-level filling factor) is observed with ρ tending to zero as T is lowered. We identify B_c^L, the point where the temperature coefficient of resistivity (TCR) changes its sign, with the critical point of the insulator-to-QH transition[2]. At still higher B, beyond the $\nu = 1$ QH state, the system turns insulating and a second T-independent transition point is seen at B_c^H. B_c^H therefore marks the critical B of the QH-to-insulator transition[15]. Following the path set by earlier studies[10,16,17] we focus, for now, on the low-B transition and follow, in Fig. 1b–e, the evolution of the critical point B_c^L as we increase p.

Data obtained from the same sample at successive increases of the hole density are shown in Fig. 1b–e. Similarly to Fig. 1a, a low-B transition point is evident in Fig. 1b, but occurs at a lower B. This trend continues in Fig. 1c until finally, in Fig. 1d, the crossing point disappears. In addition to the shift of B_c^L towards lower B, the higher p causes more QH states to become experimentally observable.

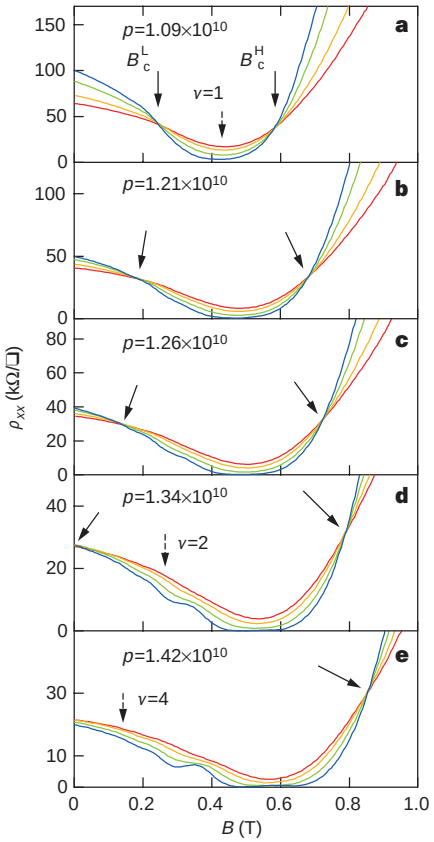

Figure 1 Isotherms of the magnetoresistance data of sample H324Bc at various hole densities. In ISIS samples, the hole carrier-density (p) is varied by applying voltage (V_g) to the grown back-gate of the ISIS. The ohmic contacts to the two-dimensional layer have to be alloyed very carefully to avoid an electrical short between this layer and the underlying gate. As a result, the use of an ISIS structure is accompanied by complications in realizing reliable ohmic contacts at extremely low ps and low Ts. In most of our devices, only some of the alloyed contacts survive at low T and low p. For the sample in this study, we do not have Hall measurements compatible with the set of measurements we present here. The sample was wet-etched to the shape of a standard 'Hall bar' (60 × 120 μm) and the measurements were done in a dilution refrigerator with a base T of 57 mK, using the a.c. lock-in technique with an excitation current of 1 nA flowing in the [01$\bar{1}$] direction. The traces are colour coded with blue being low, and red being high, temperature: values of 63, 122, 177 and 217 mK were used at each p value. The solid arrows indicate the position of the crossing points, and the dashed arrows the position of the $\nu = 1$, 2 and 4 filling factors. Resistivity along the current direction (ρ_{xx}) was measured in units of kΩ per square.